Article

Stereoselectivity and Structural Characterization of an Imine Reductase (IRED) from Amycolatopsis orientalis

Godwin A. Aleku, Henry Man, Scott P. France, Friedemann Leipold, Shahed Hussain, Laura Toca-Gonzalez, Rebecca Marchington, Sam Hart, Johan P. Turkenburg, Gideon Grogan, and Nicholas J Turner

ACS Catal., **Just Accepted Manuscript** • DOI: 10.1021/acscatal.6b00782 • Publication Date (Web): 10 May 2016

Stereoselectivity and Structural Characterization of an Imine Reductase (IRED) from *Amycolatopsis orientalis*

Godwin A. Aleku,[a†] Henry Man,[b†] Scott P. France,[a] Friedemann Leipold,[a] Shahed Hussain,[a] Laura Toca-Gonzalez [a], Rebecca Marchington [a], Sam Hart,[b] Johan P. Turkenburg,[b] Gideon Grogan[b] and Nicholas J. Turner[a]**

[a]School of Chemistry, University of Manchester, Manchester Institute of Biotechnology, 131 Princess Street, Manchester, M1 7DN, UK.

[b]York Structural Biology Laboratory, Department of Chemistry, University of York, YO10 5DD York, UK.

ABSTRACT: The imine reductase *Ao*IRED from *Amycolatopsis orientalis* (Uniprot R4SNK4) catalyzes the NADPH-dependent reduction of a wide range of prochiral imines and iminium ions, predominantly with (*S*)-selectivity and with e.e.s of up to >99%. *Ao*IRED displays up to 100-fold greater catalytic efficiency for 2-methyl-1-pyrroline (2MPN) compared to other IREDs, such as the enzyme from *Streptomyces* sp. GF3546, which also exhibits (*S*)-selectivity, and thus *Ao*IRED is an interesting candidate for preparative synthesis. *Ao*IRED exhibits unusual catalytic properties, with inversion of stereoselectivity observed between structurally similar substrates, and also, in the case of 1-methyl-3,4-dihydroisoquinoline, for the same substrate, dependent on

the age of the enzyme after purification. The structure of *Ao*IRED has been determined in an 'open' *apo*-form, revealing a canonical dimeric IRED fold in which the active site is formed between the N- and C-terminal domains of participating monomers. Co-crystallisation with NADPH gave a 'closed' form in complex with the cofactor, in which a relative closure of domains, and associated loop movements, has resulted in a much smaller active site. A ternary complex was also obtained by co-crystallization with NADPH and 1-methyl-1,2,3,4-tetrahydroisoquinoline [(MTQ], and reveals a binding site for the (*R*)-amine product which places the chiral carbon within 4 Å of the putative location of the C4 atom of NADPH that delivers hydride to the C=N bond of the substrate. The ternary complex has permitted structure-informed mutation of the active site, resulting in mutants including Y179A, Y179F and N241A, of altered activity and stereoselectivity.

KEYWORDS: Biocatalysis; Chiral Amine; Imine Reductase; Oxidoreductase; NADPH

INTRODUCTION

The asymmetric synthesis of chiral amines is of central importance to the chemical industries, as these moieties feature in a large proportion of pharmaceuticals and agrochemicals. Recently a number of approaches have been reported for the biocatalytic synthesis of chiral amines,[1] including the application of hydrolases,[2] transaminases,[3] amine oxidases[4] and amine dehydrogenases.[5-7] The direct reduction of prochiral imines by NAD(P)H-dependent oxidoreductases, termed imine reductases or IREDs, is now receiving more attention, after studies by Mitsukura and Nagasawa[8-10] demonstrated that two strains of *Streptomyces* contained NADPH-dependent oxidoreductases capable of stereocomplementary reductions of the model substrate 2-methyl pyrroline (2-MPN, **1a**, Scheme 1).

Since the initial identification of these (*R*)- and (*S*)-selective IREDs, several groups have now reported the isolation and application of further oxidoreductases from a wider subfamily that are capable of the asymmetric reduction of prochiral imine substrates with a high degree of stereoselectivity.[11-17] The latest developments in this area has been summarized in three recent reviews.[18-20] The interest in IREDs has been stimulated by the possibility that the enzymes may offer advantages of selectivity and environmentally benign methodology compared to abiotic methods of asymmetric imine reduction that employ transition metal catalysts.[21]

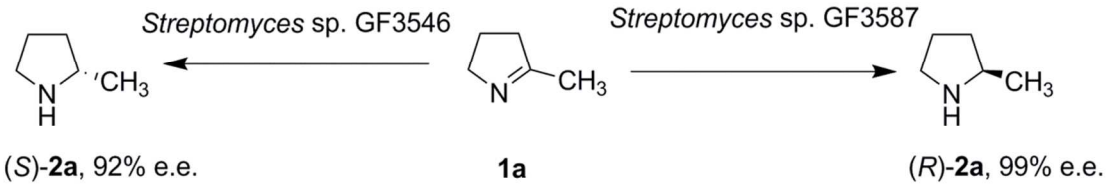

Scheme 1. Stereocomplementary reductions of 2-MPN **1a** by *Streptomyces* spp.

The mechanism of IREDs is not well understood and indeed it appears that different members of the family employ different amino acid residues within the active site for substrate recognition and/or catalysis. The first structure of an enzyme for which NADPH-dependent IRED activity towards **1a** had been demonstrated was the enzyme Q1EQE0 from *Streptomyces kanamyceticus*, which catalyzes the (*R*)-selective reduction of **1a** albeit with low activity.[16] The structure of this IRED consists of an intimate homodimer in which the two active sites are located at the interface between an N-terminal Rossman domain of one subunit, and a C-terminal helical bundle in the other. The domains in each monomer are connected by a long helix from which an aspartate residue, Asp187, protrudes into the active site, with its side chain approximately 8 Å from the C4 atom of the nicotinamide ring of NADPH that delivers and accepts hydride. The structure is most similar to an hydroxyisobutyrate dehydrogenase 2CVZ,[22] in which a lysine residue, which

superimposed with the aspartate in Q1EQE0, was suggested to be the proton donor to the nascent alcohol in the reduction of the titular substrate by that enzyme. By analogy, it was proposed that Asp187 may act as a proton donor in the reduction of imine substrates, and indeed mutation of this residue to Ala or Asn by ourselves[16] and other groups[13] in Q1EQE0 and homologs, resulted in variants with reduced catalytic activity. Interestingly, in IREDs that possess (*S*)-selectivity towards **1a**, the Asp/Lys position is occupied by a tyrosine residue, which in this case has its phenolic hydroxyl group positioned approximately 5 Å from the NADPH C4 atom, possibly as a proton donor, as has been demonstrated for the IRED pteridine reductase previously.[23] The location of this tyrosine was revealed using structures of (*S*)-selective IREDs from *Streptomyces,*[12] *Bacillus*[24] and *Nocardiopsis*[24] and its mutation to Ala[13] or Phe[24] has again been shown to diminish IRED activity in such enzymes.

Recent work by Pleiss and Hauer[13] has shown that there exists a much wider family of potential IREDs, with a range of different amino acids in the Lys/Asp/Tyr position as predicted by sequence alignments. Indeed Wetzl and co-workers[17] have recently shown that some of these homologs contain residues with aprotic side-chains, such as phenylalanine, in this position. Despite the mutational investigations at this position, the absolute requirement for a proton donor in IRED catalysis has not been clarified, as it may be that the imine substrate is already protonated in solution prior to hydride delivery. We were prompted therefore to pursue structural and mechanistic investigations of an IRED with an aprotic residue in the Lys/Asp/Tyr position, and we selected the IRED homolog Uniprot code R4SNK4 (named *Ao*IRED) from the vancomycin producer *Amycolatopsis orientalis,* which features an Asn residue in this position. Biotransformation and kinetics studies reveal *Ao*IRED to be predominantly (*S*)-selective, with superior activity to previously described (*S*)-IREDs, and also to possess surprising properties that

include inversions of stereoselectivity upon very small changes in substrate structure, and also, with four of the substrates, upon storage of the enzyme. In addition, structural investigations have yielded both an *apo*-structure and an NADPH complex, but also a ternary complex with a reaction product, (*R*)-1-methyl-1,2,3,4-tetrahydroisoquinoline [(*R*)-MTQ]. The structures have informed rational mutagenesis studies of *Ao*IRED, but also suggest a significant role for protein dynamics in catalysis by this enzyme.

RESULTS

Substrate specificity and stereoselectivity

The gene encoding *Ao*IRED was cloned and expressed in *E. coli*, and the protein purified using protocols detailed in the Supporting Information (Section S2). Following purification, the effects of pH and temperature on the activity of *Ao*IRED using **1a** as substrate were determined (Supporting Information; Section S3). The pH optimum was found to be 7.5 and the temperature optimum 50°C, although rapid denaturation was also observed at this temperature. In order to characterize the activity of *Ao*IRED with respect to substrate scope we examined a broad range of cyclic imines. When stored at 4°C at a concentration of 2 mg mL^{-1}, the enzyme retained >90% activity after 4 weeks. Examination of a series of 2-substituted pyrrolines (**1a-d**), piperideines (**3a-g**) and azepines (**5a-b**) (Scheme 2, Table 1) established that *Ao*IRED catalyzes reduction of the 2-methyl-substituted derivatives (**1a, 3a** & **5a**) predominantly to the corresponding (*S*)-amine products with excellent *e.e.*s of up to 98%.

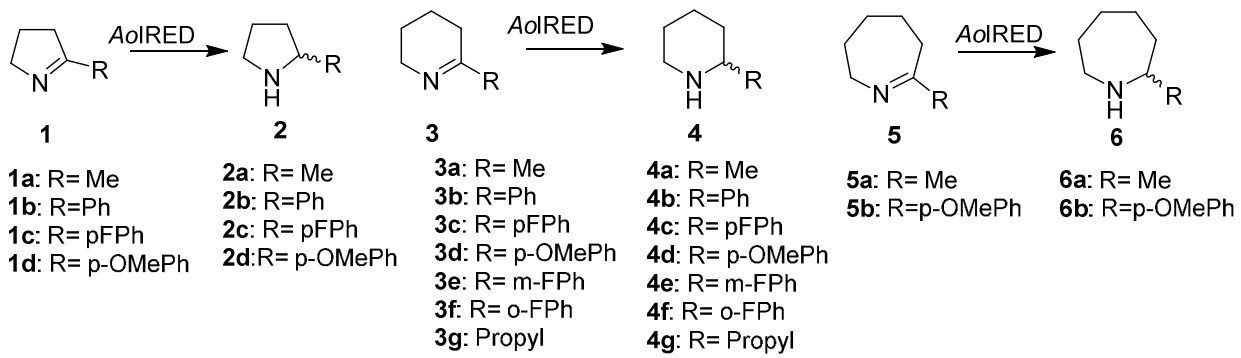

Scheme 2. Monocyclic prochiral imines reduced by fresh purified *Ao*IRED.

Table 1. Monocyclic prochiral imines reduced by fresh purified *Ao*IRED.

Substrate	Product	Conversion (%)	e.e. (%)	Absolute Configuration
1a	**2a**	96	n.d.[c]	(*S*)-
1b	**2b**	100	95	(*S*)-
1c	**2c**	98	>99	(*S*)-
1d	**2d**	85	>99	(*R*)-
3a	**4a**	>99	98	(*S*)-
3b	**4b**	>99	40	(*S*)-
3c	**4c**	>99	60	(*R*)-
3d	**4d**	77	90	(*R*)-
3e	**4e**	>99	71	(*S*)-
3f	**4f**	>99	4	(*R*)-
3g	**3g**	>99	>99	(*R*)-
5a	**6a**	95	>99	(*S*)-[a]
5b	**6b**	76	96	(-)[b]

[a]Inversion of selectivity was observed when a 24 h old aliquot of *Ao*IRED was used as the catalyst**.** Results of biotransformations using fresh purified *Ao*IRED are presented. [b] Absolute configuration not determined.[c] Lack of baseline separation prevented e.e. calculation; see Figure S7.

Interestingly, and in contrast to the selectivity pattern observed with the *Streptomyces* IREDs[10,15] the (*S*)-amine products were also preferentially formed upon reduction of 2-phenylpyrroline **1b** (95% e.e.) and 2-phenylpiperideine **3b** (40% *e.e.*), which, due to a change in Cahn-Ingold-Prelog priority, represents an actual inversion of stereoselectivity, in which hydride attacks the opposite face of the substrate. Remarkably, replacement of phenyl by a *para*-fluorophenyl **3c** or *para*-methoxyphenyl **3d** substituent on the piperideine ring led to a reversal of stereoselectivity, yielding (*R*)-**4c** (60% *e.e.*) and (*R*)-**4d** (90% *e.e.*) respectively. These results suggest that very small changes in the substrate, in this case replacement of H by F or OMe, can lead to dramatic changes in the stereoselectivity of reduction, presumably through associated changes in the substrate binding mode. Interestingly, transformation of azepine **5a** using fresh purified *Ao*IRED gave the (*S*)-amine, as shown in Table 1, but using older enzyme, the stereoselectivity was shown to invert, yielding the (*R*)-product. This phenomenon is described in more detail below.

Inversion of stereoselectivity in the reduction of 1-methyl-3,4-dihydroisoquinoline 9.

Further evidence of selectivity changes upon binding were observed when using dihydroisoquinoline and β-carboline substrates (Scheme 3, Table 2).

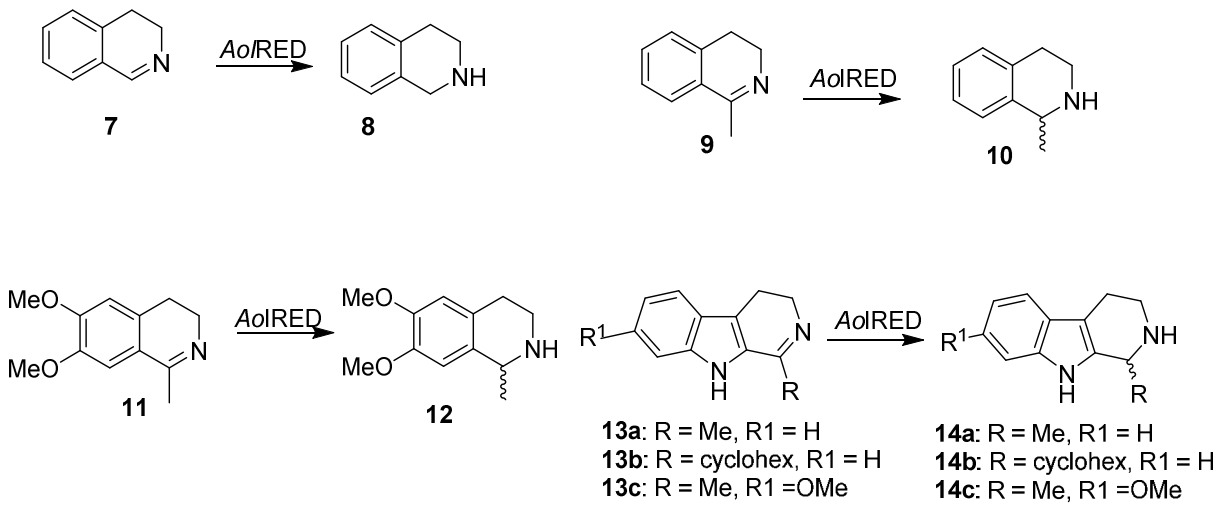

Scheme 3. Bulky prochiral imines reduced by fresh purified *Ao*IRED.

Table 2. Bulky prochiral imines reduced by fresh purified *Ao*IRED.

Substrate	**Product**	**Conversion (%)**	**e.e. (%)**	**Absolute configuration**
7	**8**	100	n/a	n/a
9	**10**	100	81	(*S*)-[a]
11	**12**	50	79	(*S*)-
13a	**14a**	5	>99	(*R*)-
13b	**14b**	66	71	(*R*)-
13c	**14c**	15	79	(*S*)-[a]

[a] Inversion of selectivity was observed when a 24 h old aliquot of *Ao*IRED was used as the catalyst**.** Results of biotransformations using fresh purified *Ao*IRED are presented. n/a= not applicable.

Thus reduction of β-carboline **13a** yielded the (*R*)-product (99% e.e.), albeit in low yield, whereas reduction of **13c**, which features a methoxy substituent on the phenyl ring, yielded the (*S*)-amine (79% *e.e.*). Even more remarkable was the reduction of 1-methyl-3,4-

dihydroisoquinoline **9**, in which the stereoselectivity of reduction was found to depend upon the form and age of the biocatalyst used. Thus a fresh lysate of cells expressing *Ao*IRED converted **9** to (*S*)-**10** (85% *e.e.*) as did fresh purified enzyme (81% *e.e.*). However, an aliquot of purified *Ao*IRED stored at 4°C for 24 h converted **9** to (*R*)-**10** (98% *e.e.*) (Figure 1). Monitoring the stereoselectivity as a function of storage time showed a steady increase in the preponderance of (*R*)-**10**, eventually leading to total inversion of enantioselectivity towards **9** with an excellent *e.e.* of 95-98% within 24 h and >99% after 14 d. Varying the reaction pH from 6-10 did not have any effect on the selectivity change. Any contribution to the effect from the recycling enzyme glucose dehydrogenase (GDH) was ruled out, as the inversion of stereochemistry was

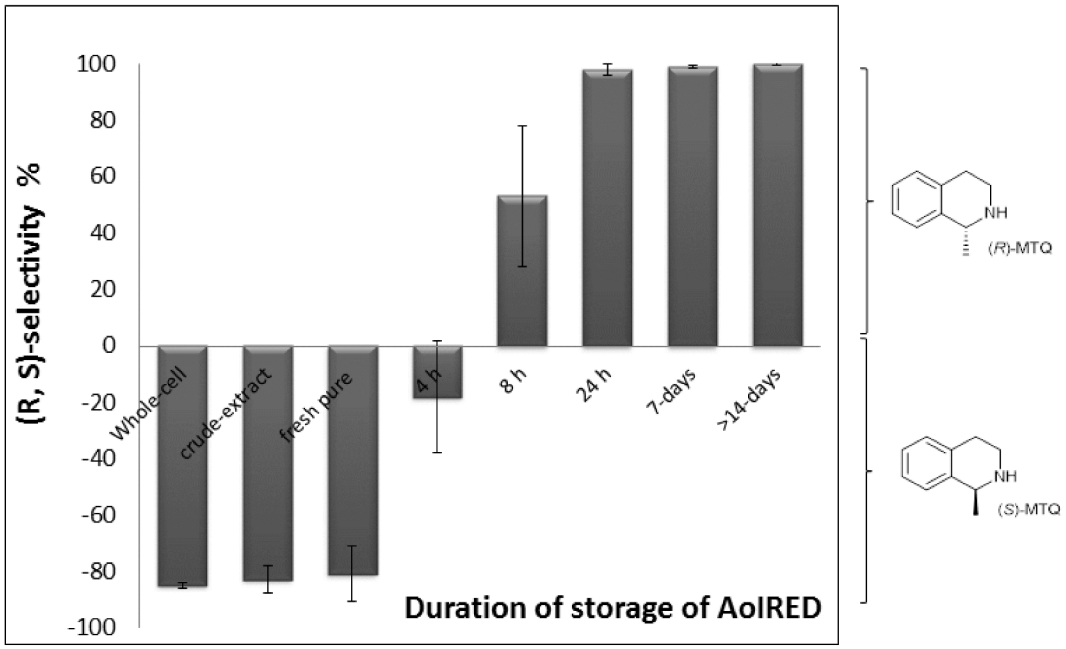

Figure 1. Selectivity switch of *Ao*IRED towards 1-methyl-3,4-dihydroisoquinoline **9**. *Ao*IRED in whole cell, fresh lysate and fresh purified form yielded (*S*)-**10**, whereas older stocks of the protein yielded (*R*)-**10**. (Experiments were repeated with three different batches of *Ao*IRED and

standard deviations are represented with error bars; On the y-axis, '-100 % e.e. indicates 100% e.e. for the (*S*)-enantiomer; '100 % e.e.' indicates 100% e.e. for the (*R*)-.

also observed when the reactions were performed with stoichiometric NADPH. The addition or removal of imidazole, which was employed in purification, and may have interfered with substrate binding, from the enzyme preparations, also did not have any effect, nor did the addition of 1-20 mM DTT, added in an effort to slow the oxidation of active site thiols. Attempts to reverse the selectivity of the older enzyme towards **9** were unsuccessful. An inversion of stereoselectivity in the KRED from *T. ethanolicus*, reported by Phillips and co-workers,[25] prompted us to study the stereoselectivity of reduction of **9** at different temperatures by 7 day old enzyme, but no effect was observed. To investigate any peptide-assisted behavior of *Ao*IRED, we incubated the purified old stock of *Ao*IRED with crude extract from *E. coli* bearing an empty pET-28a vector, using the same conditions for cultivation and induction as used in the *Ao*IRED whole-cell system, but again, no effect was observed. However, the addition of equal concentrations of bovine serum albumin (BSA) to the freshly purified *Ao*IRED was shown to slow the transformation from an (*S*)- to (*R*)-selective enzyme. A 24 h old aliquot of purified *Ao*IRED containing BSA (5-10 times the concentration of *Ao*IRED), added immediately after purification, afforded (*S*)-**10** with 76% *e.e.*, whereas a 24 h old '*Ao*IRED-only' aliquot yielded (*R*)-**10** (98% *e.e.*). Eventually, a 72 h old aliquot of '*Ao*IRED + BSA' challenged with **9** yielded (*R*)-**10** *(*e.e 98%).

Stereoselective reduction of iminium ions

Tertiary chiral amines are important structural motifs in pharmaceuticals, and could in theory be obtained through the IRED-mediated reduction of iminium ions. Indeed, recent reports by

Zheng, Xu and co-workers have demonstrated that (*R*)- and (*S*)-selective IREDs from *Paenibacillus lactis* catalyzed the reduction of indoline iminium ions with excellent stereoselectivity.[26, 27] The ability of *Ao*IRED to catalyze the reduction of iminium ions was tested using substrates **15a-15d, 17**, **19a** and **19b** (Scheme 4, Table 3). Conversions ranged from 6% for **15c** to 90% for **19a,** with good to excellent e.e.s, the best being achieved for substrates **15b** and **17**. The highest conversion obtained was for *N*-benzylated substrate **15b** and *N*-methyldihydroisoquinoline **19a**, with 79% and 90% respectively.

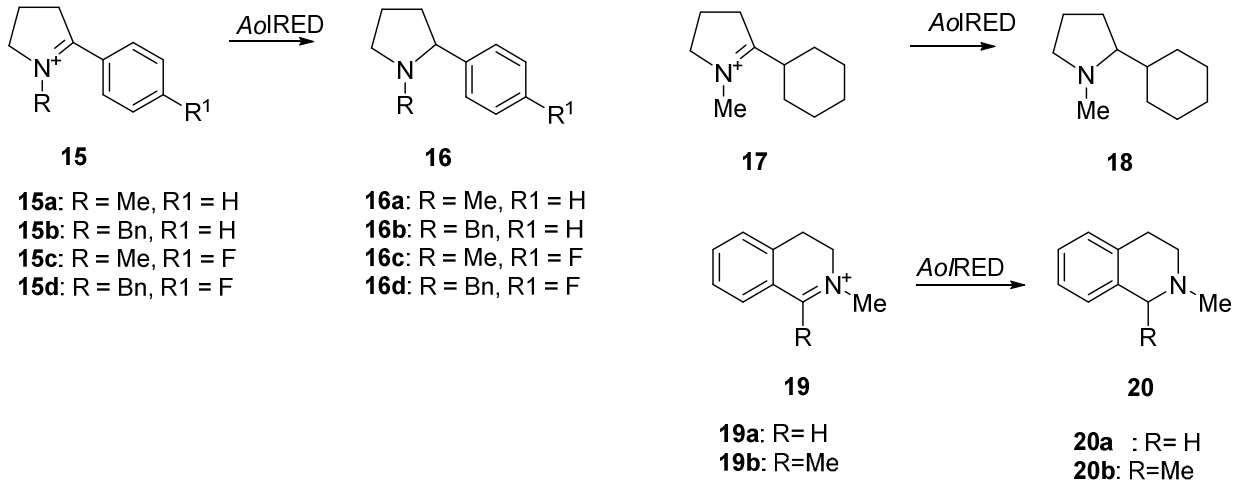

Scheme 4. Prochiral iminium ions reduced by fresh *Ao*IRED lysate.

Table 3. Prochiral iminium ions reduced by fresh *Ao*IRED lysate.

Substrate	**Product**	**Conversion (%)**	**e.e (%)**	**Absolute configuration**
15a	**16a**	8	66	(*R*)-
15b	**16b**	79	n.d.[b]	(*R*)-
15c	**16c**	6	n.d.[c]	(*R*)-
15d	**16d**	30	67	(*R*)-
17	**18**	12	90	(*R*)-
19a	**20a**	90	n/a	*n/a*
19b	**20b**	40	92	(*S*)- [a]

[a] Inversion of selectivity was observed when a 24 h old aliquot of *Ao*IRED was used as the catalyst**.** Results of biotransformations using fresh *Ao*IRED lysate are presented.[b] Lack of baseline separation prevented e.e. calculation; see Figure S19. [c] Lack of baseline separation prevented e.e. calculation; see Figure S20.

Kinetics

The determination of the kinetic parameters for representative substrates (Table 4) revealed an increasing turnover number with increasing ring size from five- (**1a**) to six membered (**3a**) rings (**1a, 3a**). The k_{cat}/K_m values for **1a** and **3a** were 0.17 s^{-1} mM^{-1} and 0.53 s^{-1} mM^{-1} respectively, which for **1a** is approximately 100-fold greater than the IRED from *Streptomyces* GF3546 (k_{cat}/K_m = 0.002 s^{-1} mM^{-1}),[11] which also possesses (*S*)-selectivity towards **1a**, revealing *Ao*IRED to be the most catalytically efficient (*S*)-selective IRED described in this class to date. The highest turnover number, and indeed the highest catalytic efficiency, for *Ao*IRED was observed with the bicyclic dihydroisoquinoline **7** (k_{cat} = 0.94 s^{-1}; k_{cat}/K_m = 2.58 s^{-1} mM^{-1}) although the superior binding affinity for a ligand was observed with the bulky 2-phenylpiperideine **3b** (K_m = 0.22 mM).

Table 4. Steady-state kinetic parameters for selected *Ao*IRED substrates.

Substrate	K_m (mM)	k_{cat} (s^{-1})	k_{cat}/K_m (s^{-1} mM^{-1})
1a	0.87 ± 0.43	0.15 ± 0.08	0.17 ± 0.18
3a	0.65 ± 0.11	0.35 ± 0.01	0.53 ± 0.11
3b	0.22 ± 0.01	0.12 ± 0.00	0.38 ± 0.08
3c	0.51 ± 0.16	0.14 ± 0.01	0.27 ± 0.07
7	0.36 ± 0.04	0.94 ± 0.01	2.58 ± 0.30
9	0.72 ± 0.05	0.74 ± 0.02	1.03 ± 0.40
19b	0.96 ± 0.11	0.77 ± 0.02	0.80 ± 0.20

Structural studies of *Ao*IRED

The structure of *Ao*IRED has been obtained in three forms: an 'open' *apo*-structure, a 'closed' NADPH complex, and a ternary complex of the 'closed' form that also features (*R*)-**10**, the product of (*R*)-selective reduction of 2-methyl-dihydroisoquinoline **9**. *Ao*IRED shares the intimately associated domain sharing dimeric structure of other IRED structures in the database (Figure 2).

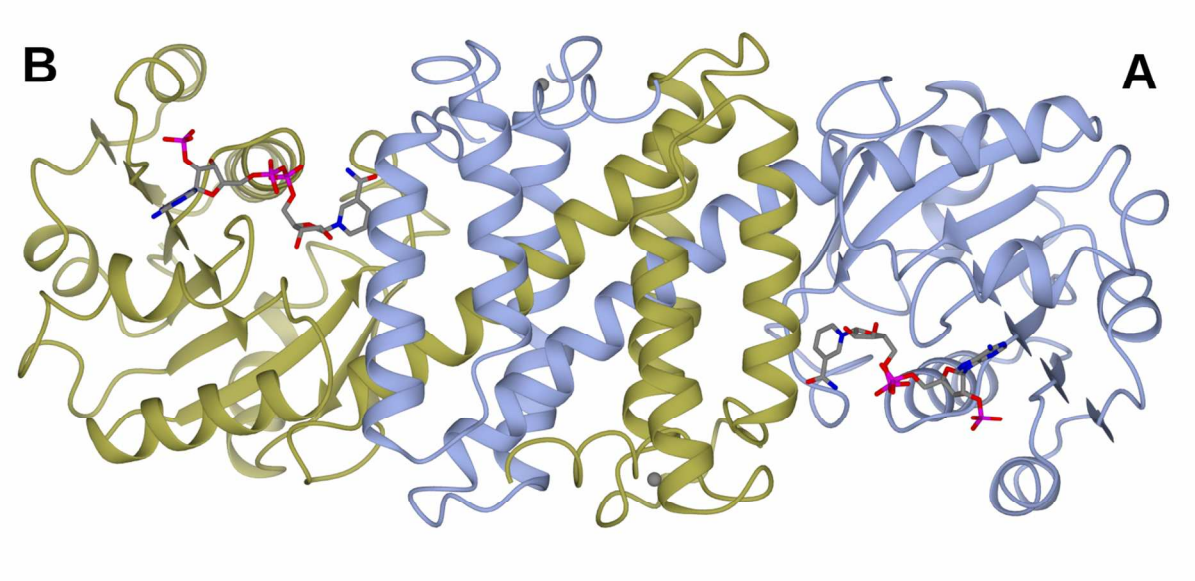

Figure 2. Dimer structure of *Ao*IRED illustrating the canonical IRED fold with domain sharing between subunits. Structure is shown in ribbon format with monomers A and B in light blue and gold. NADPH is shown in cylinder format with carbon atoms in grey, is shown at the dimer interface.

Indeed, analysis on the DALI server[28] indicated that the closest structural homolog was the (*R*)-selective Q1EQE0[16] (3ZHB; 46% amino acid sequence identity; rmsd 2.3 Å over 282 C-alpha atoms). The monomer structure adopts the canonical IRED fold now established for both (*R*)- and (*S*)-selective enzymes with a standard Rossman fold consisting of residues Thr2 to Gly 165; the transdomain helix (α8) from Leu166 to Ser194 and the C-terminal helical bundle formed from α8 and α9−α12, culminating in Arg290. A full representation of the secondary structural motifs can be found in Figure S23. Superimposition of *Ao*IRED with (*R*)-selective IRED Q1EQE0 and (*S*)-selective *Bc*SIRED revealed a very high level of conservation of structure within the Rossman fold, and indeed within the C-terminal helical bundle. Superimposition of the *apo-Ao*IRED with the *Ao*IRED-NADPH complex revealed that the loop

Thr225 to Gly236 between helices α9 and α10 displayed a remarkable 180° flip to bring the loop from beneath the C-terminal domain to occupy a position towards at the distal region of the active site cleft (Figure S24), giving a 'closed' form of the active site that is clearly reduced in volume compared to the actives site cleft in the *apo* structure. The loop movement in the NADPH complex appears to result from a 180° flip of the peptide bond between Ala 223 and Pro224. There are also substantial changes in the Rossman fold coincident with NADPH binding: the region between Leu69 and Ala78 between strand β4 and helix α4 folds over the Rossman domain with the result that the side chain of Tyr72 flips from the NADPH phosphate binding pocket on the enzyme periphery in the *apo*-structure, to the interior of the domain, where the phenolic hydroxyl now forms hydrogen bonds with the side chains of Asp118, Tyr116 and Ser96 (Figure S25). This moves the Cα and hydroxyl group of Tyr72 distances of 6 Å and 17 Å respectively. The effect is to remove the side chain of Tyr72 from the ADP binding pocket where it would occlude the binding of the adenine ring. Coincident with this large movement is the reorientation of the side chain of Arg36 in the *apo*-structure from the enzyme periphery to the ADP binding pocket, where it now interacts with the ADP ribose 2' phosphate. We have termed the structure of the *apo*- and NADPH-complex structures to be the 'open' and 'closed' forms of *Ao*IRED respectively.

Numerous approaches were taken to obtaining complexes of *Ao*IRED with imine substrate or amine products, including a range of ligands in combination with NADPH and $NADP^+$. Co-crystallization of *Ao*IRED with NADPH and *rac*-**10** yielded a ternary complex that superimposed well with the NADPH complex, with an rmsd for the subunit 'A' of 0.29 Å over 276 C-alpha atoms. The omit map at the subunit interface revealed density consistent with the presence of the (*R*)-enantiomer of MTQ, (**Figure 3**), and also for NADPH, excepting the nicotinamide riboside.

The binding of NADPH has been sufficient to close the complex around the amine ligand and this is now found parallel to the active site cleft, ideally positioned for hydride delivery from NADPH to the electrophilic carbon. The plane of the ligand is stacked against hydrophobic residues (A)Leu175 and (A)Met178 on one side of the active site, and (A)Pro124 on the other, with the nitrogen atom of (*R*)-MTQ at 3.4 Å from the amide of Asn241 and 4.4 Å from the phenol group of Tyr179. The side chain of Asn171, homologous with the Asp and Tyr residues of (*R*)- and (*S*)-selective enzymes studied previously, is relatively remote from the amine-NADPH interaction, above the aromatic ring of (*R*)-MTQ as presented in **Figure 3** at a distance of approximately 5.0 Å. Superimposition with the NADPH complex revealed that the chiral carbon of the ligand would be ideally placed at approximately 3.5 Å from the C4 atom of the nicotinamide ring of NADPH that delivers hydride to the electrophilic carbon of the C=N bond. The identification of a possible ligand-binding site in the ternary (*R*)-MTQ complex prompted us to mutate local residues in order to gauge their influence on catalytic activity.

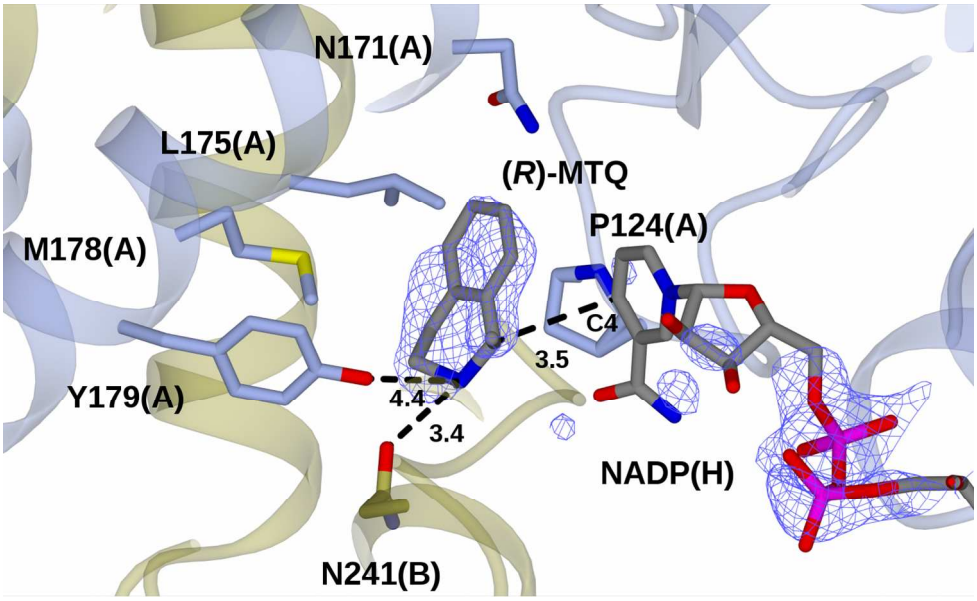

Figure 3. Detail of amine binding site in 'closed' *Ao*IRED (*R*)-MTQ ternary complex obtained through co-crystallization of *Ao*IRED with racemic MTQ and NADPH. The peptide backbone and side chain carbon atoms of monomers A and B are colored light blue and gold respectively. Electron density corresponds to the $F_o - F_c$ (omit) map contoured at a level of 2.5σ. (*R*)-MTQ atoms have been added for clarity. The omit map also features density for the ADP-ribose-2'-phosphate, but not the nicotinamide riboside, which could not be modelled. Atoms for the latter have been included for illustrative purposes using superimposition with the NADP(H) complex structure as a basis.

Site-directed mutagenesis of *Ao*IRED

In order to probe the role of various active-site residues within *Ao*IRED a series of site-directed mutagenesis experiments was performed. The structure of *Ao*IRED in complex with (*R*)-**10** suggested that some residues, such as Tyr179 and Asn241 within or near the hydrophophobic pocket opposite the NADPH-binding site may be involved in ligand recognition, especially through interactions with the nitrogen atom. These interactions were explored through the creation and assay of mutants Y179A, Y179F and N241A. The

contribution to activity of residue Asn171, the pendant residue at the top of the active site as pictured in **Figure 3**, and which corresponds to Asp187 in *Sk*IRED was also assessed through assay of mutants N171A and N171D.

Y179A and Y179F were shown to be active against a broad panel of substrates, showing high enantioselectivity in some cases, although the activity of the Y179A mutant was markedly lower towards substrates **1a, 1b, 3b and 3d** (selected data are presented in Table 5; for full details see Table S5). Stereoselectivity towards smaller substrates such as **1a** was not affected, but, notably, enantioselectivity toward 2-phenylpiperideine **3b** and bicyclic imine **11** was inverted for both Y179A and Y179F variants. The N241A mutant displayed reduced conversions to the WT for smaller substrates, but broader substrate tolerance (Table 5; Table S6). Of particular note were the reactions with substrates **11** and **13c**, all of which gave higher conversions than the WT enzyme, and with inverted stereoselectivity. In general, the N171A and N171D variants gave lower conversions than the WT enzyme, reflecting lower activity, and largely with no change in stereopreference. (Table 5; Table S7).

Table 5. Biotransformation of selected substrates by active site mutants of *Ao*IRED.

Imine	Data for *Ao*IRED variants [C (%); e.e. (%) and abs. config. amine product]					
	WT	**Y179A**	**Y179F**	**N241A**	**N171A**	**N171D**
1a	96; 82 (*S*)-	23; 99; (*S*)-	35; 47 (*S*)-	43; 81 (*S*)-	31; >99 (*S*)-	2; >99 (*S*)-
1b	100; 95 (*S*)-	8; 99 (*S*)-	99; 92 (*S*)-	43; 81 (*S*)-	100; 4, (*S*)-	100; 95 (*S*)-
3b	99; 40 (*S*)-	32; 43 (*R*)-	93; 8 (*R*)-	99; 0	41; 68 (*S*)-	80; 80 (*S*)-
3d	70; 90 (*R*)-	3; 59 (*R*)-	25; 84 (*R*)-	56; 72 (*R*)-	2; 99 (*R*)-	11; 80 (*R*)-
11	50; 79 (*S*)-	15; >99 (*R*)-	5; 99 (*R*)-	99; 85 (*R*)-	2; 31 (*S*)-	2; 99 (*S*)-
13c	15; 62 (*S*)-	10; 99 (*S*)-	9; 99 (*S*)-	96; 60 (*R*)-	18; 71 (*S*)-	6; 99 (*S*)-

Kinetic studies of variants of Y179, N241 and N171 using substrates **1a**, **7** and **9** (selected data are presented in Table 6; further data in Table S8-S10) showed that the Y179A variant displayed up to 1.6 fold improved catalytic efficiency towards dihydroisoquinolines **7** and **9,** compared to the WT, although the Y179F variant was less efficient (Table 6)**.** N241A displayed comparable kinetics overall to the WT, with slight increases in K_m. Analysis of N171A and N171D variants revealed that mutations at N171 result in higher K_m values and lower turnovers for bicyclic substrates (Table 6; Table S10), contributing to lower second-order rate constants overall, particularly for the alanine mutant.

Table 6. Kinetic parameters of active site mutants of *Ao*IRED against selected substrates

Imine		Kinetic data for *Ao*IRED variants [K_m (mM); k_{cat} (s^{-1}); k_{cat}/K_m (s^{-1} mM^{-1})][a]				
	WT	**Y179A**	**Y179F**	**N241A**	**N171A**	**N171D**
1a	0.87; 0.15; 0.17	1.77; 0.03; 0.05	0.87; 0.01; 0.02	1.27; 0.22; 0.17	7.90; 0.12; 0.02	2.22; 0.17; 0.01
7	0.36; 0.94; 2.58	0.39; 1.52; 3.95	0.85; 0.32; 0.38	0.47; 0.95; 2.02	1.90; 0.15; 0.08	1.44; 0.15; 0.10
9	0.72; 0.74; 1.03	0.45; 0.92; 2.03	0.19; 0.07; 0.36	0.83; 0.76; 0.92	3.15; 0.01; 0.01	0.72; 0.21; 0.30

[a] Errors have been omitted from this Table for reasons of space, but can be found in relevant Tables in the SI.

DISCUSSION

*Ao*IRED is an active imine reductase with a broad substrate spectrum and the potential to serve as a valuable asymmetric catalyst with certain substrates, including 5- (**1b-1d**), 6- (**3a**, **3d**) and 7- (**5a**) membered moncyclic imines, as well as isoquinolines such as **9** and some iminium ion substrates. However, the situation is complicated by the observation with *Ao*IRED, but also other IREDs,[17,24] of small changes in substrate structure having major changes on stereochemical preference. *Ao*IRED appears to display a mixed stereopreference for substrates that is difficult to visualize, as CIP priority changes render the use of '*re*-/*si*-' and '*R*/*S*' terminology confusing. Scheme 5 shows that one set of substrates, exemplified by **1a**, **2a** and **3d** are attacked by hydride at the prochiral face of the molecule with the imine bond on the right-hand side of the nitrogen atom; conversely, the second set of substrates, represented by **3b**, **3c** and **9 (**by stored *Ao*IRED) are attacked on the prochiral face with the imine bond on the left-hand side of the nitrogen atom.

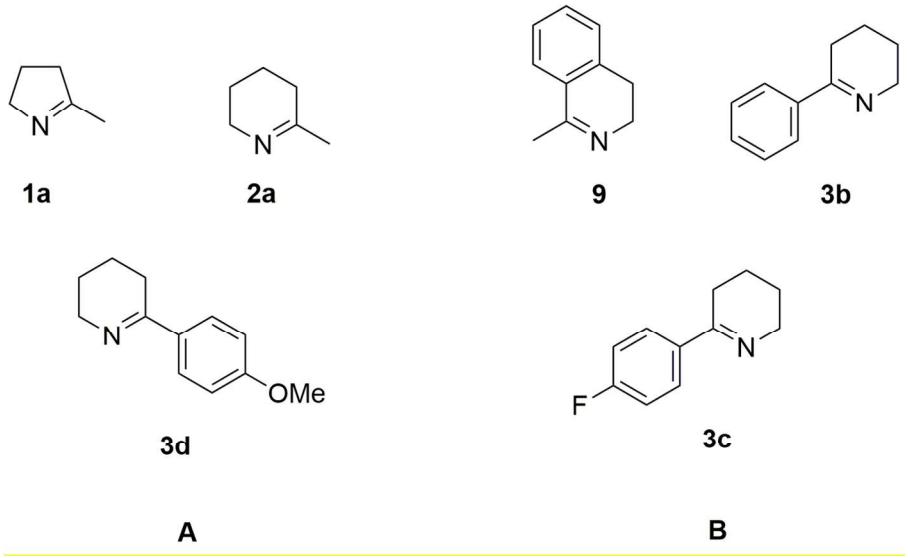

Scheme 5. Two sets of prochiral imines representative of alternate stereochemical outcomes in reductions by *Ao*IRED. The NADPH hydride attacks compounds grouped **A** or **B** from the front of the page in each case.

Even the very small changes in structure between **3d** and **3b** require that *Ao*IRED must invert the substrate to present the opposite face to the nicotinamide ring for the attack of hydride at the electrophilic carbon of the C=N bond. This may implicate the use of more than one binding mode, or even binding site, for different substrates. A multiplicity of binding modes is also one possible explanation suggested by the remarkable inversion of stereoselectivity observed for the reduction of substrate **9** on storage of the enzyme, and the plasticity of the active site suggested by structural studies may also play a role in the complex behavior observed.

An extreme example of the unusual stereoselective properties of *Ao*IRED is the inversion of stereopreference in the reduction of 1-methyl-3,4-dihydroisoquinoline **9**. Both fresh lysate and fresh purified *Ao*IRED catalyzed the formation of the (*S*)-amine product **10**, but storage yielded an enzyme that catalyzed the formation of the (*R*)- enantiomer. Despite many investigations, it

did not prove possible to reverse this effect, although BSA was shown to slow the transformation from an (*S*)- to an (*R*)- selective enzyme. BSA is known to stabilize the conformation of proteins including dehydrogenases through hydrophobic effects[29] and also to alter kinetic and thermodynamic parameters through molecular crowding,[30] although we are unaware of any associated effects on the stereoselectivity of enzymes. Possible explanations for the observed inversions of stereoselectivity could therefore include conformational changes or changes in protein oligomerization on storage, but also possibly changes in the hydration of the active site cleft, which have been observed by Phillips to invert the enantioselectivity of the KRED from *T. ethanolicus*.[31] Given the time scale of the conformational change, X-ray crystallographic studies have not been able to shed light on the phenomenon of inverted stereoselectivity, but do provide information on some of the mobile elements in *Ao*IRED.

The structures of *Ao*IRED suggest that multiple conformations of the enzyme are indeed to be encountered along the reaction coordinate, with major loop reorganisations observed on cofactor binding. Some of this mobility, such as the movement of the tyrosine loop in the N-terminal domain, may be general, as this tyrosine is observed in all currently known IRED structures. The loop movements beneath the active site in *Ao*IRED, however, may be restricted to closely related homologs, as there is clearly some diversity in IRED sequences in this region. This loop movement, in conjunction with the relative closure of the two domains that participate in active site formation, serves to close the active site to form a pocket that is much reduced in volume compared to the active site cleft that has been observed in IRED structures previously, and in which cofactor and substrate can interact for the reduction reaction. One abiding mystery of IRED catalysis is the ability of stereocomplementary enzymes to catalyze the production of antipodal amine products using apparently large active site clefts that appear to be fairly similar

in nature. The observation of the smaller closed active site in the *Ao*IRED ternary complex suggests a ligand recognition site, at least in this enzyme, that is now small enough to possibly exert control over which prochiral face of the imine is presented to the hydride.

In the time taken to acquire pure *Ao*IRED and to crystallize it, it is probable that the form of the enzyme in crystallization drops is the (*R*)-selective form, and, indeed it is the (*R*)- enantiomer of **10** that is found in the ternary complex structure obtained by co-crystallizing *Ao*IRED with NADPH and racemic **10**. This complex placed cofactor, amine and active site in context, and allowed a structure-guided approach to the possible roles of residues through mutational analysis. Although N241 especially appears to interact directly with the nitrogen atom of the amine product, it cannot act as a general acid in protonation of the reaction intermediate. Indeed the imine substrate is probably protonated at the pH values used for bioconversions, so such protonation may not be necessary. However, it may act as an anchor for the nitrogen atom that fixes the ligand for reduction at the *si*- face of the substrate in this case. Mutation of N241 to alanine resulted in slight increases in the K_m for **1**, **7** and **9**, and also created a more efficient enzyme for the transformation of large substrates such as **11** and **13c**, although its effect on enantioselectivity was mixed, dependent on the substrate. In the same region, mutation of Y179, which makes more distant contact with the amine nitrogen, to alanine actually created a more efficient biocatalyst for the transformation of bicyclic imines. Together these residues may be interesting targets for future mutational studies designed to expand the substrate spectrum of *Ao*IRED.

In the ternary complex structure Asn171, equivalent to Asp and Tyr residues previously mooted to have roles in catalysis on the basis of homology to aldehyde dehydrogenase enzymes, is somewhat remote from the interaction between cofactor and amine in the active site. While we

cannot exclude a role in mechanism for the equivalent residue in other IREDs, certain homologs such as *Ao*IRED clearly exist which have no requirement for a protic residue in this position for catalysis. Mutation of Asn171 to Asp certainly did not increase *Ao*IRED activity and, indeed, mutation to either Asp or Ala gave variants of higher K_m and slightly altered stereoselectivity, possibly suggesting a partial role for Asn171 in early substrate recognition in *Ao*IRED as it approaches the site of reduction.

CONCLUSION

*Ao*IRED represents an interesting new addition to the library of IRED catalysts for applications in asymmetric synthesis. Previous studies suggest that these enzymes are applicable in either whole-cell reactions, in which substrate concentrations of up to 25 mM have been used,[15] or as isolated enzymes, for which established methods of nicotinamide cofactor recycling can be applied.[11] However, the studies of *Ao*IRED again reveal that stereochemical control in these enzymes is complex and the prediction of selectivity is especially difficult, and has to be investigated on a case-by-case basis. However, the description of a ternary complex of an IRED does provide new avenues for mutation directed at altering the substrate scope of this enzyme, and the mutations of Tyr179 and Asn241 suggests that this may be possible, with the increased activity towards certain substrates engendered by this mutation. It is certain that further structural and mechanistic studies will be required to shed more light on mechanism and stereoselectivity and IREDs, and that the determinants of each may be different for subgroups of IREDs bearing different amino acids within their active sites.

EXPERIMENTAL SECTION

Chemicals

Commercially available chemicals and reagents were purchased from Sigma-Aldrich (Poole, Dorset, UK), Prozomix (Haltwhistle, Northumberland, UK), Alfa Aesar (Karlsruhe, Germany) and Acros Organics (Geel, Belgium) unless stated otherwise. HPLC solvents were obtained from Sigma-Aldrich (Poole, Dorset, UK) or ROMIL (Waterbeach, Cambridge, UK) and GC gases from BOC gases (Guildford, UK). Further general information is given in the Supporting Information (Section S1). 2-Methyl-1-pyrroline (**1a**), 2-methylpiperidine (**4a**), harmaline (**13c**) and 3,4-dihydroisoquinoline (**7**) were purchased from Sigma-Aldrich (Poole, Dorset, UK). 2-Methylpyrrolidine (**2a**), 1-methyl-3,4-dihydroisoquinoline hydrochloride (**9**), 1-methyl-6,7-dimethoxy-3,4-dihydroisoquinoline (**11**) and 6,7-dimethoxy-1-methyl-1,2,3,4-tetrahydro-isoquinoline hydrochloride (**12**) were sourced from Acros Organics (Geel, Belgium), 2-phenylpyrrolidine (**2b**) was purchased from Apollo Scientific (Stockport, UK) and 1-methyl-1,2,3,4 tetrahydroisoquinoline (**10**) was obtained from GlaxoSmithKline (Stevenage, UK). Compounds **3a-3d**, **3g**, **4a-4d**, **4g**, **5a** & **5b**, **6a** & **6b, 13a** & **13b** and **14a** and **14b** were synthesised according to previously reported methods.[11,11,15] Procedures for the preparation of **3e, 3f, 4e, 4f, 15a-15d**, **16a-16d**, **17**, **18**, **19a**, **19b**, **20a** and **20b** and their characterization data are included in the Supporting Information (Section S4).

Gene synthesis, cloning, expression and protein purification

General information on strains and plasmids, and details of gene design and cloning protocols can be found in the Supporting Information (Section S2). The codon-optimized gene sequence encoding *Ao*IRED was synthesized by Biomatik (Cambridge, Ontario, Canada) and sub-cloned into pET28a-(+) vector using *Nde*I and *Xho*I restriction sites to form pET 28a-His-*Ao*IRED plasmid (Figure S1). Site-directed mutants of *Ao*IRED were generated using the Stratagene QuikChange site directed mutagenesis protocol, using primers as listed in the Supporting

Information (Section S2). The presence of mutations in all constructs was verified by sequencing. Production of *Ao*IRED was achieved in *E. coli* BL21 (DE3) which had been transformed with the recombinant *Ao*IRED plasmid. Cultivation was performed in 500 mL lysogeny broth (LB) medium (1% tryptone, 0.5% yeast extract, 1% NaCl) with kanamycin (30 μg mL^{-1}) added as the antibiotic marker. Cultures were initially incubated at 37°C with shaking at 250 r.p.m. At an optical density (OD_{600nm}) of between 0.6 and 0.8, isopropyl β-D-1-thiogalactopyranoside (IPTG) was added to a final concentration of 0.2 mM to induce the expression of *Ao*IRED. Incubation was continued at 30°C and 250 r.p.m. for 18 h. Cells were then harvested by centrifugation and resuspended in sodium phosphate buffer (100 mM, pH 7.5). Celles were disrupted using a Soniprep150 ultrasonicator (MSE, London, UK), employing 3 x 30 s bursts with 30 s intervals at 4°C. Cell debris was removed by centrifugation, after which the resulting supernatant was loaded onto a 5 mL His-Trap HP column (GE healthcare). The protein was eluted using a gradient of 0-300 mM imidazole in sodium phosphate buffer (100 mM, pH 7.5) containing 300 mM NaCl. The purified enzyme was desalted using 30 kDa cut-off Centricon filters (15 mL), and washed twice with sodium phosphate buffer (100 mM, pH 7.5) to remove NaCl and imidazole. For protein for crystallisation, further purification by size exclusion chromatography (SEC) using a HiLoad 16/60 Superdex 75 PrepGrade (GE Healthcare) gel filtration column was performed. *Ao*IRED was purified by SEC with Tris-HCl buffer (50 mM, pH 8.0) containing 500 mM NaCl. SEC trace (Figure S2) and SDS-PAGE analysis (Figure S3) can be found in the Supporting Information (Section S2). The protein concentration was determined using Bradford assay against BSA as a concentration standard.

Biotransformations

Whole cell biotransformation reactions typically contained *E.coli* BL21(DE3) resting cells containing expressed *Ao*IRED (OD_{600nm} of 50), 2 % (v/v) dimethylformamide, 5 mM imine substrate and 50 mM glucose in sodium phosphate buffer (100mM, pH 7.5). Reactions were incubated at 30°C with shaking at 250 r.p.m. for 18 h.

Biotransformations using isolated enzymes were performed with purified *Ao*IRED employing glucose dehydrogenase (GDH)/NADPH as a cofactor recycling system. A typical 500 μL reaction mixture contained 20 mM D-glucose, 0.2 mg mL^{-1} GDH, 0.3 mM $NADP^+$, 0.4 mg mL^{-1} *Ao*IRED 5 mM imine/iminium ion substrate and 2% (v/v) dimethyl formamide. The reaction volume was made up to 500 μL with sodium phosphate buffer (100mM, pH 7.5). Reactions were incubated at 30°C with shaking at 250 r.p.m. shaking for 18 h, after which they were quenched by the addition of 30 μL of 10 M NaOH and extracted twice with 500 μL *tert*-butyl methyl ether. The organic fractions were combined and dried over anhydrous $MgSO_4$ and analyzed on HPLC or GC using chiral columns. Details of columns and analytical methods, with chromatograms, can be found in the Supporting Information (Section S5).

Enzyme Assays

The imine-reducing activity of *Ao*IRED was measured by monitoring the oxidation of NADPH using a Cary 300 UV-Vis spectrophotometer (Agilent, Santa Clara, CA, USA). The consumption of NADPH was monitored at 340 (ε=6.22 mM^{-1} cm^{-1}) or 370 nm (ε=2.216 mM^{-1} cm^{-1}). The assay mixture in sodium phosphate buffer (100mM, pH 7.5) contained an imine substrate in concentrations of up to 30 mM, NADPH at concentration of 160 μM (340 nM) or 300 μM (370 nm), 1 % (v/v) DMSO and 10-50 μg of pure enzyme, in a total volume of 1000 μL. Control reactions without substrate featuring the same reaction conditions were run to determine the background consumption of NADPH. The reaction was initiated upon the addition

of purified *Ao*IRED to the mixture. A unit of *Ao*IRED was equal to the amount of the pure enzyme required to consume 1 μmol NADPH/ $NADP^+$ per min. Activity measurements were performed in triplicate and kinetic constants were determined through nonlinear regression based on Michaelis–Menten kinetics (QtiPlot software).

Protein Crystallization

Pure *Ao*IRED was subjected to crystallization trials using a range of commercially-available screens in 96-well sitting-drop format, in which each drop consisted of 150 nL protein and 150 nL of precipitant reservoir solution. The best hits for *apo*-*Ao*IRED were found in conditions containing 0.2 M calcium acetate, 0.1 M Tris pH 9.0, 8% (w/v) PEG 550 monomethyl ether (MME) and 8% (w/v) PEG 20K with protein at a concentration of 20 mg mL^{-1}. Larger crystals for diffraction analysis using optimized conditions were prepared using the hanging-drop method in 24-well plate Linbro dishes with 2 μL drops consisting of 1:1 ratio of mother liquor to protein. The best crystals were obtained in conditions containing 0.2 M calcium acetate, 0.1 M Tris pH 9.0, 8% (w/v) PEG 550 MME and 8% (w/v) PEG 20K with protein at a concentration of 20 mg mL^{-1}.

Co-crystallization of *Ao*IRED with NADPH (10 mM) did not yield crystals under the same buffer conditions. In order to obtain the NADPH complex of *Ao*IRED, native crystals were transferred from the growth drop into a cryogenic solution which consisted of the mother liquor containing ethylene glycol [20% (v/v)] and NADPH (10 mM), and incubated for 5 min, after which they were immediately flash-cooled in liquid nitrogen.

Crystals of *Ao*IRED complexed with (*R*)-**10** in the 'closed' conformation were obtained by subjecting pure *Ao*IRED to crystallization trials using a range of commercially available screens in sitting-drop format with 1 mM NADPH and 1 mM *rac*-**10** added into the mother liquor 1 h

prior to dispensing 150 nL protein and 150 nL of precipitant reservoir solution. The best hits for *Ao*IRED complexed with (*R*)-**10** were found in conditions containing 0.2 M lithium sulfate, 0.1 M BisTris pH 6.5, 25% (w/v) PEG 3350, 1 mM NADPH and 1 mM *rac*-**10** with protein at a concentration of 25 mg mL^{-1}. Larger crystals for diffraction analysis using optimised conditions were prepared using sitting-drop format 48-well MRC MAXI crystallization plates with 1 μL drops consisting of 1:1 ratio of mother liquor to protein. The best crystals were obtained in conditions containing 0.25 M lithium sulfate, 0.1 M BisTris pH 6.5, 23% (w/v) PEG 3350, 1 mM NADPH and 1 mM *rac*-**10**. The *Ao*IRED complex with (*R*)-**10** in the 'closed' conformation was obtained by soaking the pre-complexed crystals with compound NADPH and *rac*-**10** for 5 min prior to flash-cooling with liquid nitrogen without the addition of further cryoprotectants.

All crystals were tested for diffraction in-house using a Rigaku Micromax-007HF fitted with Osmic multilayer optics and a Marresearch MAR345 imaging plate detector. Those crystals that diffracted to a resolution of equal to, or better than, 3 Å resolution were retained for dataset collection at the Diamond Light Source synchrotron.

Data Collection, Structure Solution, Model Building and Refinement

Complete datasets described in this report were collected at Diamond Light Source, Didcot, Oxfordshire, U.K. The *apo*-*Ao*IRED dataset was collected on beamline I03, the NADPH complex on beamline I04 and the 'closed' (*R*)-MTQ complex on beamline I02 utilizing 10% beam transmission and helical data collection.[32] Data were processed and integrated using XDS[33] and scaled using SCALA[34] included in the Xia2 processing system.[35] Data collection statistics are given in the Supporting Information in Table S4. The crystals of *apo*-*Ao*IRED in the 'open' form were in space group $C222_1$. The crystals of the 'closed' complexes were in group $P2_12_12_1$. The structure of *Ao*IRED was solved with MOLREP[36] using a monomer model of the IRED

Q1EQE0, PDB code 3ZGY. The solution(s) in $C222_1$ contained one molecule in the asymmetric unit; those in $P2_12_12_1$ contained two monomers, representing one dimer. The solvent content in the *apo*-, NADPH complex and 'closed' (*R*)-MTQ complex were 52.4%, 42.8% and 40.5% respectively. The structures were built and refined using iterative cycles in Coot[37] and REFMAC,[38] the latter employing local NCS restraints. For the NADPH complex of *Ao*IRED, following building and refinement of the protein and water molecules, clear residual density was observed in the omit maps at one of the subunit dimer interfaces. This was modelled and refined as NADPH. For the ternary complex, clear density was observed in the relevant binding pocket that could be modelled as (*R*)-MTQ. The MTQ coordinate and refinement library file were prepared using PRODRG.[39] All structures were finally validated using PROCHECK.[40] Refinement statistics for all structures are presented in Table S4. The Ramachandran plot for the apo-*Ao*IRED showed 97.5% of residues to be situated in the most favored regions, 2.1% in additional allowed and 0.4% residues in outlier regions. For the NADPH complex, the corresponding values were 96.0%, 3.1% and 0.9% respectively and for the 'closed' (*R*)-MTQ complex, 97.3%, 2.3% and 0.4% respectively. The coordinates and structure factors have been deposited in the Protein Databank with the accession codes 5a9r, 5a9s and 5fwn respectively.

ASSOCIATED CONTENT

Synthesis of substrates and product standards; Cloning, expression and mutation protocols; Details of Analytical protocols including chiral HPLC and GC traces of products ; X-ray crystallography data; pH and temperature optima studies; Tables of mutant kinetic data. This material is available free of charge via the Internet at http://pubs.acs.org.

AUTHOR INFORMATION

Corresponding Authors

[a]School of Chemistry, University of Manchester, Manchester Institute of Biotechnology, 131 Princess Street, Manchester, M1 7DN, UK.

[b]York Structural Biology Laboratory, Department of Chemistry, University of York, YO10 5DD York, UK.

*(G.G.) Email: gideon.grogan@york.ac.uk

*(N.J.T.) Email: nicholas.turner@manchester.ac.uk

AUTHOR CONTRIBUTIONS

G.A.A, ‡ H.M., ‡ S.P.F., L.T.G., R.M., S.H. and F.L. performed experiments; ‡These authors contributed equally. S.H. and J.P.T collected X-ray crystal data; G.G. and N.J.T. designed experiments and wrote the paper.

FUNDING SOURCES

We thank the industrial affiliates of the Centre of Excellence for Biocatalysis, Biotransformations and Biomanufacture (CoEBio3) for awarding studentships to G.A.A. and H.M. S.P.F. received support from BBSRC and Pfizer for a CASE studentship. S.H. was supported by a CASE studentship from EPSRC and AstraZeneca. F.L. received support from the Innovative Medicines Initiative Joint Undertaking under the grant agreement no. 115360 (Chemical manufacturing methods for the 21st century pharmaceutical industries, CHEM21), resources of which are composed of financial contribution from the European Union's Seventh Framework Program (FP7/2007-2013) and EFPIA companies' in-kind contributions. NJT acknowledges the Royal Society of a Wolfson Research Merit Award.

ABBREVIATIONS

IRED (Imine Reductase); 2-MPN (2-methyl pyrrolidine); GDH (glucose dehydrogenase); PEG (polyethylene glycol); MME (monomethyl ether).

REFERENCES

(1) Höhne, M.; Bornscheuer, U.T. *Chemcatchem* **2009**, 1, 42-51.

(2) Buchholz, S.; Gröger, H. *Biocatalysis in the Pharmaceutical and Biotechnology Industries*; Patel, R. Ed; CRC Press: Florida, U.S.A.; **2006**; pp 829-847.

(3) Mathew, S.; Yun, H. *ACS Catal*. **2012**, 2, 993-1001.

(4) Ghislieri, D.; Green, A.P.; Pontini, M.; Willies, S.C.; Rowles I.;, Frank, A.; Grogan, G.; Turner, N.J. *J. Am. Chem. Soc.* **2013**, *135*, 10863-10869.

(5) Abrahamson, M.J.; Vázquez-Figueroa, E.; Woodall, N.B.; Moore, J.C.; Bommarius, A.S.; *Angew. Chem. Int. Ed.* **2012**, *51*, 3969-3972.

(6) Mutti, F. G.; Knaus, T., Scrutton, N. S., Breuer, M., Turner, N. J., *Science*, **2015**, *349*, 1525-2529.

(7) Chen F-F.; Liu, Y-Y.; Zheng, G-W.; Xu, J-H. *Chemcatchem*, **2015**, *7*, 3838-3841.

(8) Mitsukura, K.; Suzuki, M.; Tada, K.; Yoshida, T.; Nagasawa, T. *Org. Biomol. Chem.* **2010**, *8*, 4533-4535.

(9) Mitsukura, K.; Suzuki, M.; Shinoda, S.; Kuramoto, T.; Yoshida, T.; Nagasawa, T. *Biosci. Biotechnol. Biochem.* **2011**, *75*, 1778-1782.

(10) Mitsukura, K.; Kuramoto, T.; Yoshida, T.; Kimoto, .; Yamamoto, H.; Nagasawa, T. *Appl. Microbiol. Biotechnol.* **2013**, *97*, 8079-8086.

(11) Leipold, F.; Hussain, S.; Ghislieri, D.; Turner, N.J. *Chemcatchem* **2013**, *5*, 3505-3508.

(12) Huber, T.; Schneider, L.; Präg, A.; Gerhardt, S.; Einsle, O.; Müller, M. *Chemcatchem* **2014**, *6*, 2248-2252.

(13) Scheller, P.N.; Fademrecht, S.; Hofelzer, S.; Pleiss, J.; Leipold, F.; Turner, N.J.; Nestl, B.M.; Hauer, B. *Chembiochem* **2014**, *15*, 2201-2204.

(14) Gand, M.; Müller, H.; Wardenga, R.; Höhne M. *J. Mol. Catal. B-Enzym.* **2014**, *110*, 126-132.

(15) Hussain, S.; Leipold, F.; Man, H.; Wells, E.; France, S.; Mulholland, K.R.; Grogan, G.; Turner, N.J. *Chemcatchem*, **2015**, *7,* 579-583.

(16) Rodríguez-Mata, M.; Frank, A.; Wells, E.; Leipold, F.; Turner, N.J.; Hart, S.; Turkenburg, J.P.; Grogan, G. *Chembiochem* **2013**, *14*, 1372-1379.

(17) Wetzl, D.; Berrera, M.; Sandon, N.; Fishlock, D.; Ebeling, M.; Műller, M.; Hanlon, S.; Wirz, B.; Iding, H. *Chembiochem*, **2015**, *16*, 1749-1756.

(18) Schrittweiser, J.; Velikogne, S.; Kroutil, W. *Adv. Synth. Catal.*, **2015**, *357*,1655-1685.

(19) Grogan, G.; Turner N.J. *Chem. Eur. J.* **2016**, *22*, 1900-1907.

(20) Leipold, F.; Hussain, S.; France, S.P.; Turner, N.J. Imine reductases, In *Biocatalysis in Organic Synthesis*, Faber, K.; Fessner, W.; Turner N. Eds., *Science of Synthesis Reference Library*, Thieme Verlag, Stuttgart, New York. **2015**, *2*, pp 359-381.

(21) Fleury-Brégeot, N.; de la Fuente, V.; Castillón, S.; Claver, C.; *Chemcatchem*, **2010**, *2*, 1346-1371.

(22) Lokanath, N.K.; Ohshima, N.; Takio, K. Shiromizu, I.; Kuroishi, C.; Okazaki, N.; Kuramitsu, S.; Yokoyama, S.; Miyano, M.; Kunishima, N. *J. Mol. Biol.* **2005**, *352*, 905-917.

(23) Gourley, D.G.; Schuttelkopf, A.W.; Leonard, G.A.; Luba, J.; Hardy, L.W.; Beverley, S.M.; Hunter, W.N. *Nat. Struct. Mol. Biol.* **2001**, *8*, 521-525.

(24) Man, H.; Wells, E.; Hussain,S.; Leipold, F.; Hart, S.; Turkenburg, J.P.; Turner, N.J.; Grogan, G. *Chembiochem* **2015**, *16*, 1052-1059.

(25) Pham, T.; Phillips, R.S.; Ljungdahl, L.G. *J. Am. Chem. Soc.*, **1989**, *111*, 1935-1936.

(26) Li, H.; Luan, Z-J.; Zheng, G-W.; Xu, J-H. *Adv. Synth. Catal*. **2015**, *357*, 1692-1696.

(27) Li, H.; Zhang, G-X.; Li, L-M.; Ou, Y-S.; Wang, M-Y.; Li, C-X.; Zheng, G-W.; Xu, J-H. *Chemcatchem*. **2016**, *8*, 724-727.

(28) Holm, L.; Rosenström, P. *Nucleic Acids Res.* **2010,** *38*, 545-549.

(29) Grosch, J-H.; Loderer, C.; Jestel, T.; Ansorge-Schumacher, M.; Spieß, A.C., *J. Mol. Catal.-B Enzym.*, **2015**, *112*, 45-53.

(30) Olsen, S.N. *Thermochim. Acta*, **2006**, *448*, 12-18.

(31) Patel, J.M.; Philips, R.S., *ACS Catal*., **2014**, *4*, 692-694.

(32) Flot, D. *J. Synch. Rad.,* **2010**, *17*, 107-118

(33) Kabsch, W. *Acta Crystallogr. Sect. D. Biol. Crystallogr.* **2010**, *66*, 125-132.

(34) Evans, P. *Acta Crystallogr. Sect. D. Biol. Crystallogr.* **2006**, *62*, 72-82.

(35) Winter, G. *J. Appl. Cryst*., **2010**, *3*, 186-190.

(36)Vagin, A.; Teplyakov, A. *J. Appl. Crystallogr.* **1997**, *30*, 1022-1025.

(37) Emsley, P.; Cowtan, K. *Acta Crystallogr., Sect D: Biol. Crystallogr.* **2004**, *60*, 2126-2132.

(38) Murshudov, G.N.; Vagin, A.A.; Dodson, E.J. *Acta. Crystallogr. Sect. D. Biol. Crystallogr.* **1997**, *53*, 240-255.

(39) Schüttelkopf, A.W.; van Aalten, D.M.F. *Acta Crystallogr. Sect. D. Biol. Crystallogr*, **2004**, *60* 1355–1363.

(40) Laskowski, R.A.; Macarthur, M.W.; Moss, D.S.; Thornton, J.M. *J. Appl. Crystallogr.* **1993**, *26*, 283–291.

Table of Contents Graphic and Synopsis

The stereoselectivity of the Imine Reductase from *Amycolatopsis orientalis* (*Ao*IRED) was observed to hinge upon small changes in substrate structure, and also, in one case, on the age and state of the biocatalyst. Comprehensive activity screening, combined with structural studies, suggest that complex factors, including protein dynamics and substrate structure, combine to deliver different stereochemical outcomes for closely related imines.

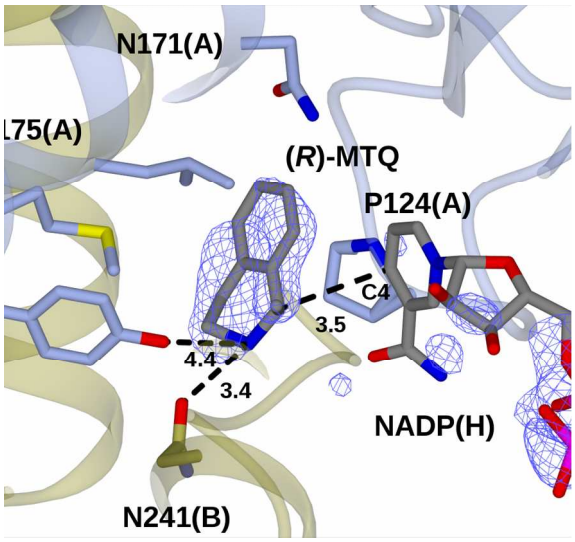

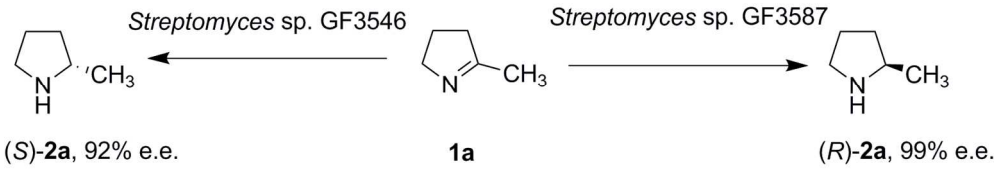

Scheme 1. Stereocomplementary reductions of 2-MPN 1a by Streptomyces spp.
147x25mm (300 x 300 DPI)

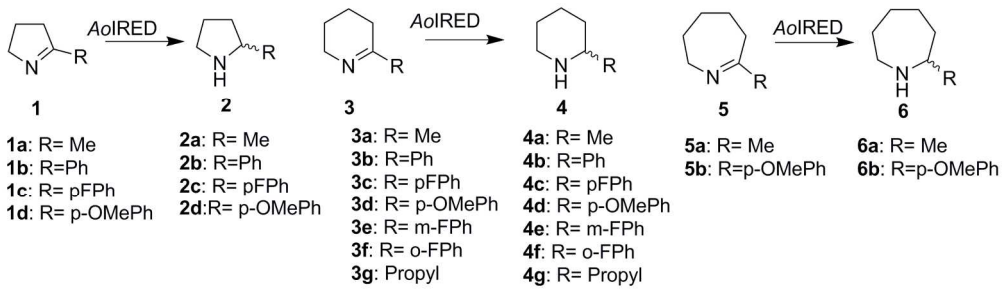

Scheme 2. Monocyclic prochiral imines reduced by purified AoIRED.
181x52mm (300 x 300 DPI)

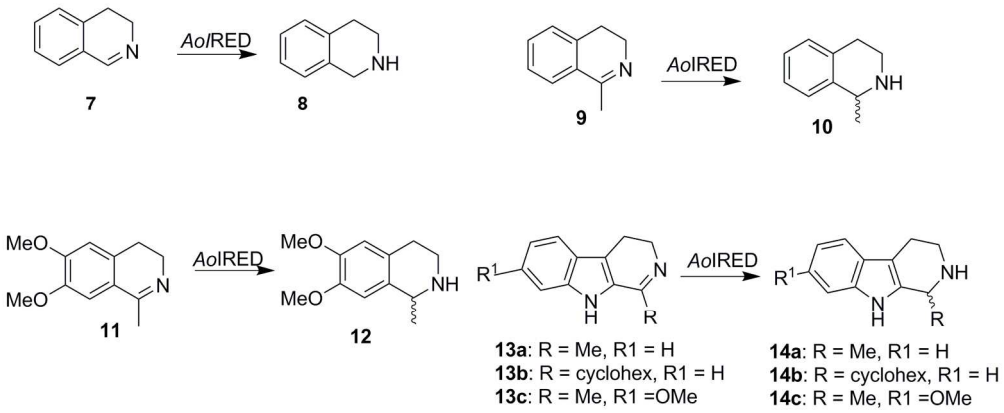

Scheme 3. Bulky prochiral imines reduced by purified AoIRED.
180x73mm (300 x 300 DPI)

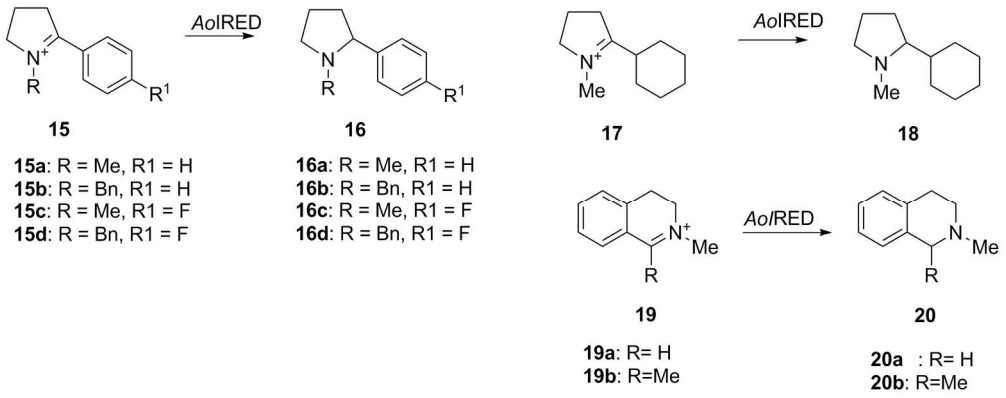

Scheme 4. Prochiral iminium ions reduced by purified AoIRED lysate.
180x71mm (300 x 300 DPI)

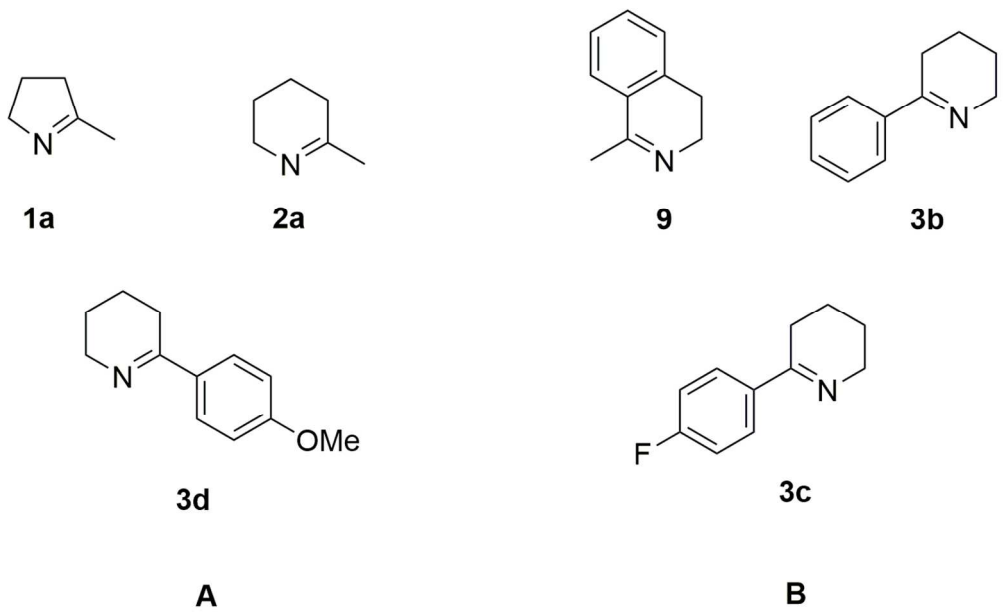

Scheme 5. Two sets of prochiral imines representative of alternate stereochemical outcomes in reductions by AoIRED. The NADPH hydride attacks compounds grouped A or B from the front of the page in each case.
119x73mm (300 x 300 DPI)

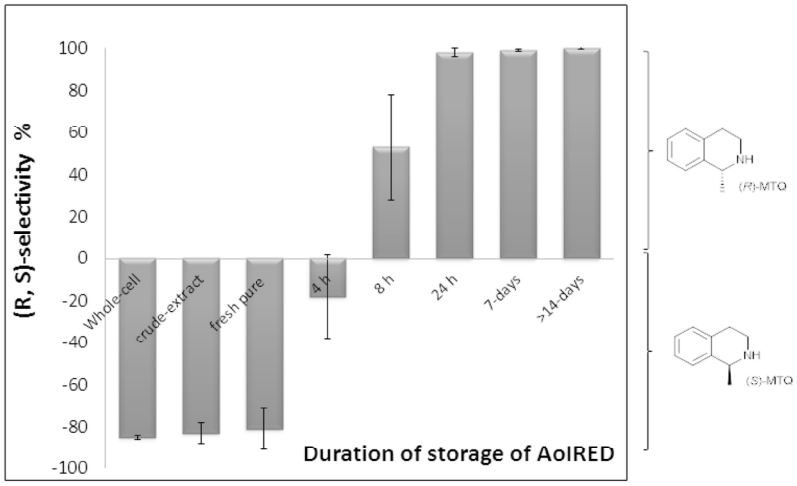

Figure 1. Selectivity switch of AoIRED towards 1-methyl-3,4-dihydroisoquinoline 9. AoIRED in whole cell, fresh lysate and fresh purified form yielded (S)-10, whereas older stocks of the protein yielded (R)-10. (Experiments were repeated with three different batches of AoIRED and standard deviations are represented with error bars; On the y-axis, '-100 % e.e. indicates 100% e.e. for the (S)-enantiomer; '100 % e.e.' indicates 100% e.e. for the (R)-.
150x112mm (300 x 300 DPI)

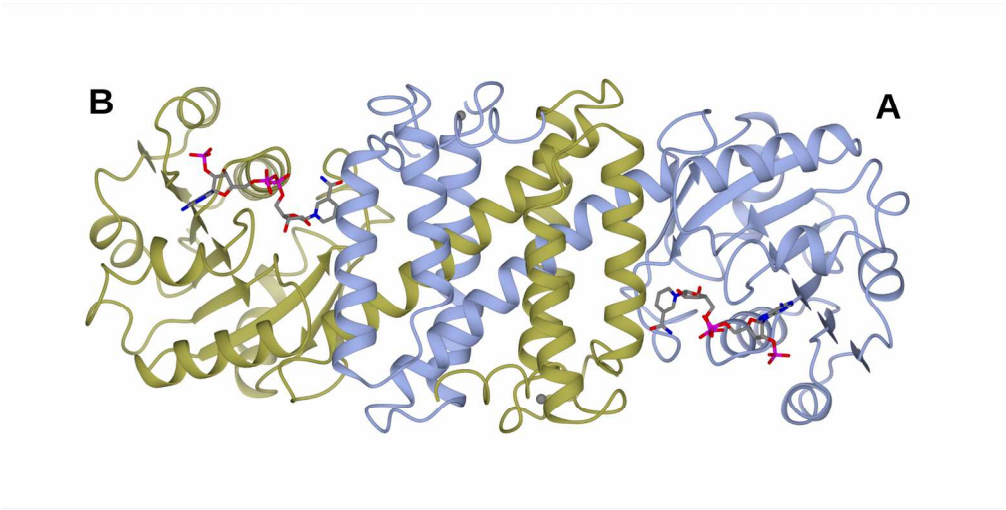

Figure 2. Dimer structure of AoIRED illustrating the canonical IRED fold with domain sharing between subunits. Structure is shown in ribbon format with monomers A and B in light blue and gold. NADPH is shown in cylinder format with carbon atoms in grey, is shown at the dimer interface.
155x78mm (300 x 300 DPI)

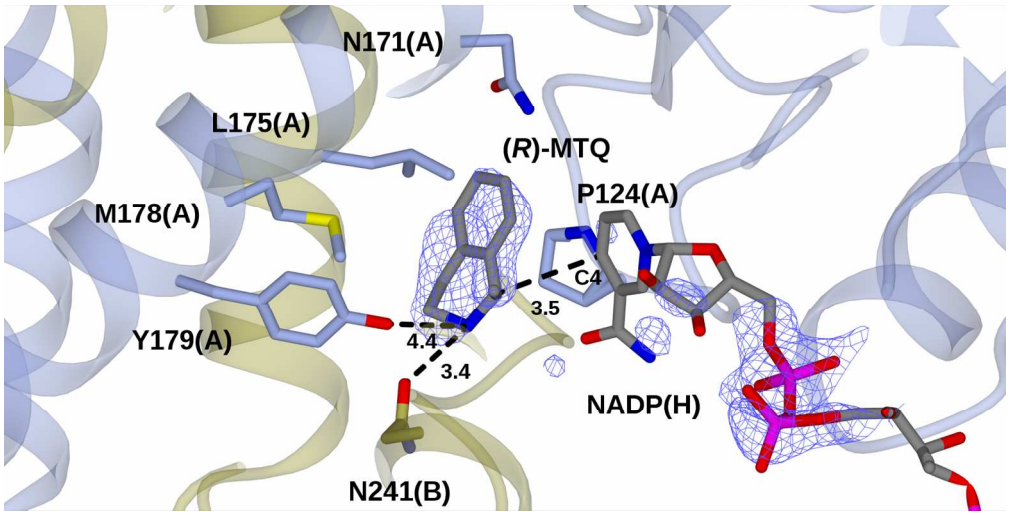

Figure 3. Detail of amine binding site in 'closed' AoIRED (R)-MTQ ternary complex obtained through co-crystallization of AoIRED with racemic MTQ and NADPH. The peptide backbone and side chain carbon atoms of monomers A and B are colored light blue and gold respectively. Electron density corresponds to the Fo – Fc (omit) map contoured at a level of 2.5σ (R)-MTQ atoms have been added for clarity. The omit map also features density for the ADP-ribose-2'-phosphate, but not the nicotinamide riboside, which could not be modelled. Atoms for the latter have been included for illustrative purposes using superimposition with the NADP(H) complex structure as a basis.
155x78mm (300 x 300 DPI)